Hue University Journal of Science: Natural Science; ISSN 1859-1388

Vol. 127, No. 1A, 2018, P. 43-53; DOI: 10.26459/hueuni-jns.v127i1A.4777

INVESTIGATION OF EXCITATION AND EMISSION PROPERTIES OF FLUORESCENCE COMPOUNDS BY DFT AND TD-DFT METHODS

Le Thi My Hoang[1], Doan Thanh Nhan[2], Mai Van Bay[2,3], Nguyen Thi Ai Nhung[4], Nguyen Khoa Hien[5], and Duong Tuan Quang[2*]

[1] Quy Nhon University
[2] University of Education, Hue University
[3] University of Education, The University of Danang
[4] University of Sciences, Hue University
[5] Mientrung Institute for Scientific Research, Vietnam Academy of Science and Technology

Abstract. The density functional theory and time-dependent density functional theory methods were used for the investigation of the excitation and emission properties of some fluorophores. The calculations were based on the optimized geometries of ground states and excited states at the B3LYP functional and LanL2DZ basis set. The results clarified the nature of the optical properties of the compounds and agreed well with experimental data. The calculated values of excitation energies and emission energies of the compounds were higher than the experimental values. These large errors occurred when there were great variations between the optimized geometries of the ground state and excited states. They could be due to the presence of components of solvent in a real solution that stabilized the excited states, leading to reduce the excitation and emission energies in the experiments.

Keywords: TD-DFT, fluorescence, absorption, emission, coumarin

1 Introduction

Fluorescence compounds are often referred to as fluorophores. Their molecules typically contain a π-electron conjugated system, including aromatic groups [1]. They can be excited by the absorption of a photon and return to the ground state with an emission of fluorescence [2].

Fluorophores play an important role in many fields. They are used as an analytical tool to determine the concentrations of various species. The fluorescent analysis method has been attracting the attention of scientists. This is due to the fact that it is often sensitive to the analytes and easy to carry out. Especially, it can be used to monitor the substances in living cells [3, 4]. Fluorescence is also used as a powerful tool in biochemistry and biotechnology fields. It is used for studying the structure and dynamics of matter or living systems at a molecular or supramolecular level [5]. Besides, fluorescence is used as a

** Corresponding: duongtuanquang@dhsphue.edu.vn*

Submitted: 13-4-2018; Revised: 29-4-2018; Accepted: 3-5-2018

research tool in many fields of medical sciences. It is a promising diagnostic technique with a high sensitivity and selectivity for microorganisms-associated diseases diagnosis such as bacteria, viruses, fungi and parasites [6].

The investigation of the absorption and emission properties of a fluorophore is very important and necessary to study its applications. Currently, this process is mainly based on experimental investigations, usually requires to use a lot of chemicals, and not always successful. Meanwhile, the quantum chemical calculation can predict many important physical and chemical properties of biological and chemical systems [7–10]. However, the calculation-based investigations of the absorption and emission properties of fluorophores have been rarely reported [6].

Herein, we present the investigation of the excitation and emission properties of some fluorophores (Fig. 1) by using the time-dependent density functional theory (TD-DFT). In particular, this study is based on the calculations from the optimized geometry of the ground state and the electronically excited states. The results showed that the calculations agreed well with the previously published experimental data, and the TD-DFT method could be used well for the investigation of the optical properties of fluorophores.

2 Computational methodology

The quantum chemical calculations were performed using the Gaussian 09 program package [11]. The density functional theory (DFT) was used for the calculations of the optimization geometries and single point energies of the compounds at the S_0 ground state (GS). Meanwhile, the optimization geometries and single point energies of the compounds at the singlet excited states (EES), such as S_1, S_2, were carried out by using the time-dependent density functional theory [3, 12, 13]. The time-dependent density functional theory was also used to investigate the excitation and emission properties based on the optimized geometries of GS and EES. The difference between the energy of the S_1 state (or the S_2 state) and the S_0 state at the GS optimized geometry (R^{GS}) was considered to be the vertical absorption energy from S_0 to S_1 (or S_0 to S_2). Meanwhile, the vertical fluorescence energy from S_1 to S_0 (or S_2 to S_0) was obtained from the difference between the energy of the S_1 state (or the S_2 state) and the S_0 state at the EES optimized geometry (R^{EES}) [14, 15]. All calculations were performed at the B3LYP/LanL2DZ level theory [16, 17].

3 Results and discussion

3.1 Optimized geometries of the ground and electronically excited states

The optimized geometries GS and EES of molecular structures (I), (II), (III), (IV) and (V) are presented in Fig .2, Fig. 3, Fig. 4, Fig. 5, and Fig. 6.

For structure (I), the calculated results showed that there was no significant difference between the optimized geometries of S_0, S_1 and S_2, except some bonds of the O11, C2, C1 and C6 atoms. The O11–C2 bond lengths in S_0 and S_1 were 1.25 and 1.27 Å, respectively, equivalent to the length of the O=C double bond (1.26 Å). Meanwhile, the O11–C2 bond length in S_2 was 1.39 Å, equivalent to the length of the O–C single bond (1.43 Å). The C1–C2 bond lengths in S_0 and S_1 were 1.44 and 1.42 Å, respectively, equivalent to the length of the C–C bond in benzene (1.40 Å). Meanwhile, the C1–C2 bond length in S_2 was 1.37 Å, equivalent to the length of the C=C double bond (1.36 Å). The C1–C6 bond length in S_0 was 1.38 Å, equivalent to the length of the C=C double bond (1.36 Å). Meanwhile, the C1–C6 bond lengths in S_1 and S_2 were 1.42 and 1.46 Å, respectively, equivalent to the length of the C–C bond in benzene (1.40 Å).

For structure (II), the calculated results also showed that there was no significant difference between the optimized geometries of S_0, S_1 and S_2, except some bonds of the C1, C2, C4, C5 and C6 atoms. The lengths of the C1–C2 bond in S_0, C5–C6 bond in S_0, C4–C5 bonds in S_1 and S_0 were 1.45–1.46 Å, slightly longer than that of the C–C bond in benzene (1.40 Å). The lengths of the C1–C2 bonds in S_1 and S_2, C1–C6 bonds in S_1 and S_2, C5–C6 bonds in S_1 and S_2 were 1.42–1.43 Å, equivalent to the length of the C–C bond in benzene (1.40 Å). Meanwhile, the C1–C6 bond length in S_1 was 1.38 Å, equivalent to the length of the C=C double bond (1.36 Å).

There were significant differences in the optimized geometries of the S_0, S_1 and S_2 states of structures (III), (IV), and (V). For structure (III), the coumarin moiety and acryloxy moiety were almost in the same plane in the S_0 state, but they were almost in two planes perpendicular to each other in the S_1, S_2 states. The O15–C14–C8–C9 dihedral angles in the S_1, S_2 states were 69.8° and 61.4°, while this dihedral angle was 0.0° in the S_0 state. By contrast, for structures (IV) and (V), the coumarin moiety and acryloxy moiety were almost in the same plane in the S_2 state, but they were almost in two planes perpendicular to each other in the S_0, S_1 states. The O15–C14–C8–C9 dihedral angles in the S_0, S_1 states of structures (IV) and (V) were –47.1°; –64.1° and –49.4°; –43.3°, respectively; while these dihedral angles were –1.9° and –3.6° in the S_2 states of structures (IV) and (V), respectively. The dihedral angle twisting might cause the abnormal fluorescent characteristics in structures (III), (IV) and (V).

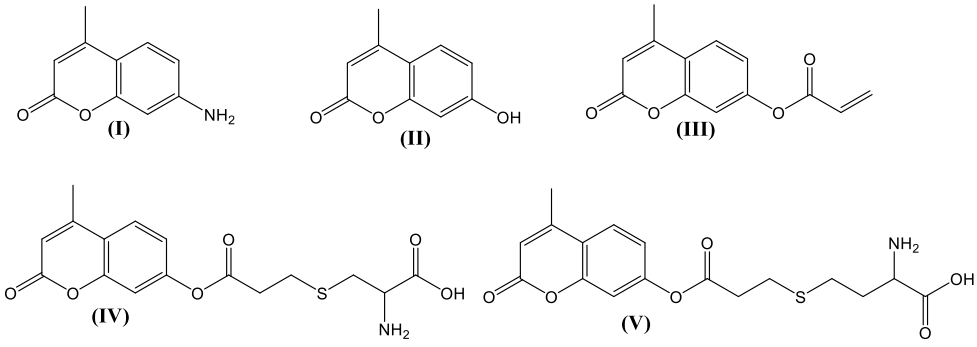

Fig. 1. Molecular structures

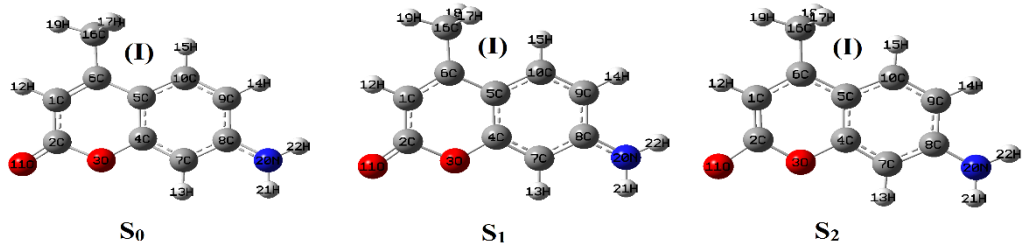

Fig. 2. GS and EES optimized geometries of (**I**)

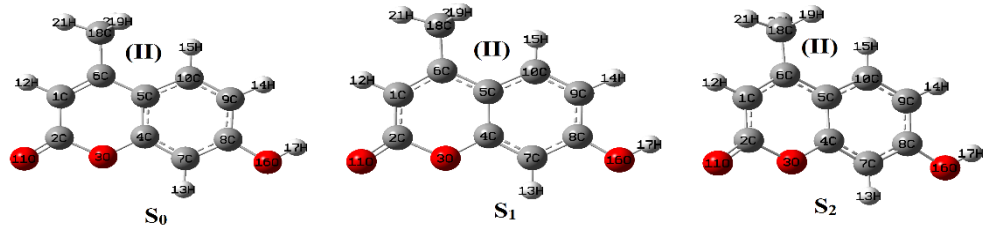

Fig. 3. GS and EES optimized geometries of (**II**)

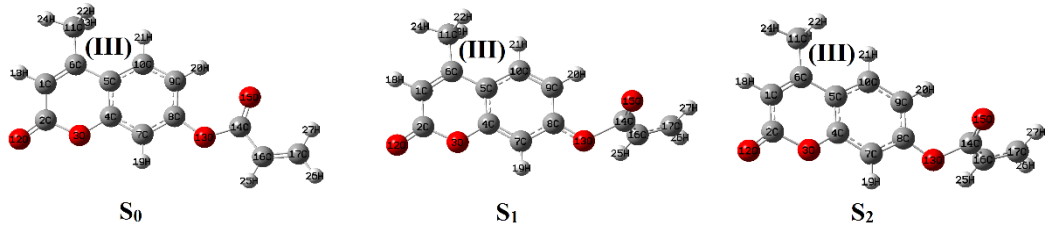

Fig. 4. GS and EES optimized geometries of (**III**)

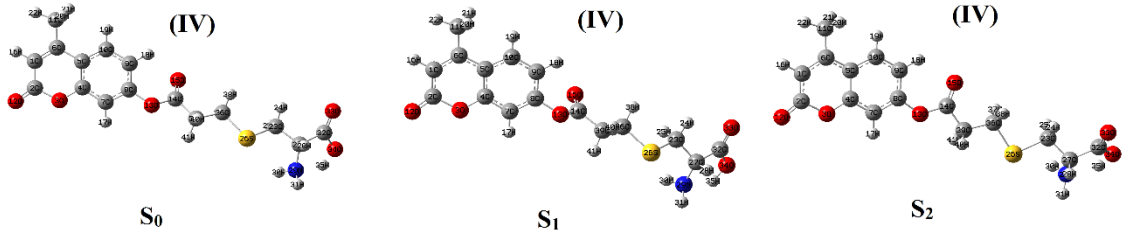

Fig. 5. GS and EES optimized geometries of (**IV**)

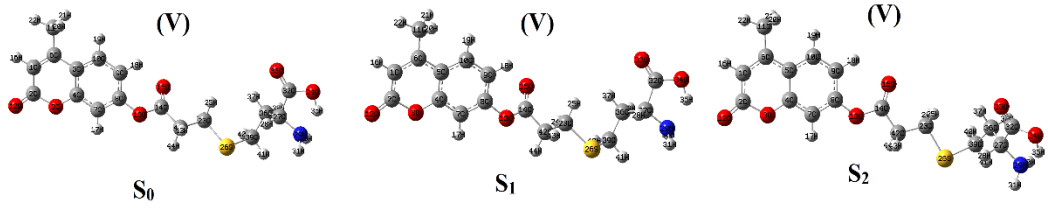

Fig. 6. GS and EES optimized geometries of (**V**)

3.2 Excitation and emission properties

The energy of the excitation and emission processes of structures (I), (II), (III), (IV), and (V) were calculated using the TD-DFT method, and their diagrams are presented in Fig. 7 to Fig. 11.

For structures (I), the calculated results showed that the $S_0 \rightarrow S_1$ transition (process (1) in Fig. 7) was the main singlet electronic transition from the ground state to the excited states with an oscillator strength (*f*) of 0.4198, much stronger than that of the $S_0 \rightarrow S_2$ transition (process (2) in Fig. 7) and other transitions. The $S_0 \rightarrow S_1$ transition was contributed by the orbital transition from HOMO to LUMO with a percentage contribution of 96.9%. The calculated results of the difference between the energy of the S_1 state and the S_0 state at R^{GS} (in water solution) showed that the vertical excitation energy of $S_0 \rightarrow S_1$ transition was 3.58 eV. According to the previously published experimental data, the excitation energy of (I) in the water solution was 3.65 eV [18]. The results showed that the calculations agreed well with experiments. For the de-excitation processes, the value of oscillator strength (*f*) of the $S_1 \rightarrow S_0$ transition at $R^{EES(S2)}$ (process (5) in Fig. 7) was very high (0.4579). However, the geometry of the S_1 state at $R^{EES(S2)}$ was not optimized yet. It quickly goes to the optimized geometry at $R^{EES(S1)}$. Therefore, the $S_1 \rightarrow S_0$ transition at $R^{EES(S2)}$ was almost non-existent. The value of oscillator strength (*f*) of the $S_1 \rightarrow S_0$ transition at $R^{EES(S1)}$ (process (3) in Fig. 7) was 0.4158, much larger than that of the remaining transitions. This is the main singlet electronic transition from EES to GS at $R^{EES(S1)}$ and contributed by the orbital transition from LUMO to HOMO with a percentage contribution of 97.1%. The calculated fluorescence energy of the $S_1 \rightarrow S_0$ transition in the water solution was obtained from the difference between the energy of the S_1 state and the S_0 state at $R^{EES(S1)}$ (process (3) in Fig. 7). It was 3.38 eV, while the previously published experimental value was 2.83 eV [18]. There was a difference of *ca*. 0.55 eV between the calculated fluorescent energy and the experimental fluorescent energy.

The calculated results from structure (II) were completely similar to those from structure (I). The $S_0 \rightarrow S_1$ transition (process (1) in Fig. 8) was a main singlet electronic transition from GS to EES and mainly contributed by the orbital transition from HOMO to LUMO with a percentage contribution of 95.6%. The calculated vertical excitation energy of the $S_0 \rightarrow S_1$ transition (in the methanol solution) was 4.02 eV, a difference of about 0.56 eV compared with the previously published experimental data [19]. The $S_1 \rightarrow S_0$ transition at $R^{EES(S1)}$ (process (3) in

Fig. 8) was a main singlet electronic transition from EES to GS and contributed by the LUMO→HOMO transition with a percentage contribution of 96.6%. The calculated fluorescence energy of the $S_1 \rightarrow S_0$ transition (in the methanol solution) was 2.64 eV, a difference of about 0.60 eV compared with the previously published experimental data [20].

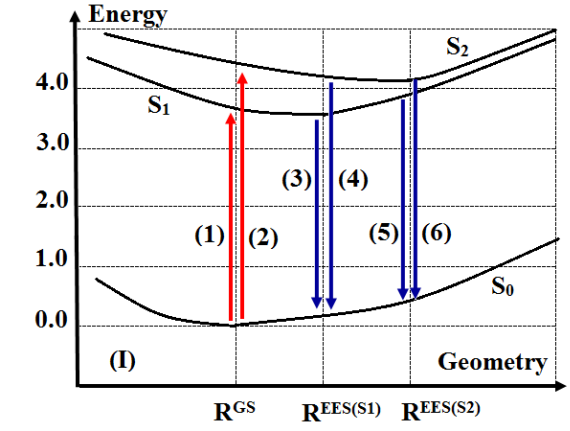

(1):E=3.58 eV, f=0.4198
(2):E=4.33 eV, f=0.0103
(3):E=3.38 eV, f=0.4158
(4):E=4.14 eV, f=0.0241
(5):E=3.33 eV, f=0.4579
(6):E=3.42 eV, f=0.0000

Fig. 7. Energy diagram of the excitation and emission processes of (I) at R^{GS}, $R^{EES(S1)}$ and $R^{EES(S2)}$ (in water solution)

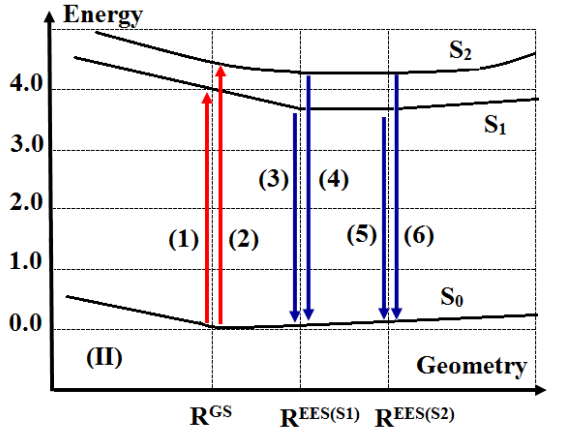

(1):E=4.02 eV, f=0.3932
(2):E=4.38 eV, f=0.0059
(3):E=3.69 eV, f=0.4201
(4):E=4.13 eV, f=0.0120
(5):E=3.69 eV, f=0.4201
(6):E=4.13 eV, f=0.0118

Fig. 8. Energy diagram of the excitation and emission processes of (II) at R^{GS}, $R^{EES(S1)}$ and $R^{EES(S2)}$ (in methanol solution)

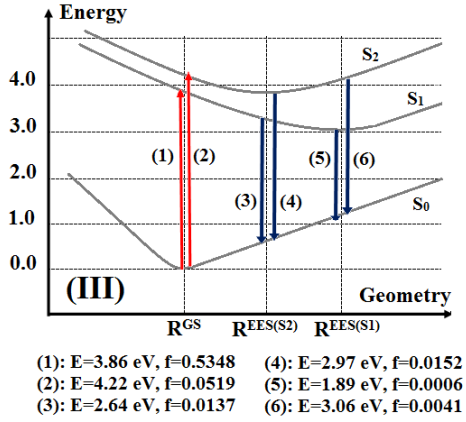

Fig. 9. Energy diagram of the excitation and emission processes of (III) at R^{GS}, $R^{EES(S1)}$ and $R^{EES(S2)}$ (in ethanol solution)

For structure (III), the $S_0 \rightarrow S_1$ transition (process (1) in Fig. 9) was a main singlet electronic transition from GS to EES and mainly contributed by the HOMO→LUMO transition with a percentage contribution of 96.21%. The calculated vertical excitation energy of the $S_0 \rightarrow S_1$ transition (in the ethanol solution) was 3.86 eV and agreed well with the previously published data that the excitation energy of (III) in the water solution was 3.87 eV [3]. For the de-excitation processes, the values of oscillator strength (*f*) of the $S_1 \rightarrow S_0$ transition and the $S_2 \rightarrow S_0$ transition at $R^{EES(S1)}$ (process (5) and (6) in Fig. 9) were very small (0.0006 and 0.0041). In addition, the lack of overlapping between the two MOs in each transition made these transitions strongly forbidden. The values of oscillator strength (*f*) of the $S_1 \rightarrow S_0$ transition and the $S_2 \rightarrow S_0$ transition at $R^{EES(S2)}$ (process (3) and (4) in Fig. 9) were larger (0.0137 and 0.0152). In addition, there was an overlapping of the MOs in these transitions. These results showed that the $S_1 \rightarrow S_0$ transition and the $S_2 \rightarrow S_0$ transition at $R^{EES(S2)}$ occur in structure (III). The calculated fluorescence energies of these transitions (in ethanol solution) were 3.49 and 3.64 eV, a difference of about 0.74 and 0.34 eV compared with the previously published data. The small values of oscillator strength (*f*) of the $S_1 \rightarrow S_0$ transition and the $S_2 \rightarrow S_0$ transition at $R^{EES(S2)}$ agreed well with the weak fluorescence intensity of structure (III) in the experiments [3].

For structure (IV), the $S_0 \rightarrow S_2$ transition (process (2) in Fig. 10) was a main singlet electronic transition from GS to EES and mainly contributed by the HOMO-1→LUMO transition with a percentage contribution of 89.17%. The calculated vertical excitation energy of the $S_0 \rightarrow S_2$ transition (in the ethanol solution) was 4.12 eV, a difference of about 0.25 eV compared with the previously published data [3]. The values of oscillator strength (*f*) of the $S_1 \rightarrow S_0$ transitions at $R^{EES(S2)}$ and $R^{EES(S1)}$ (process (3) and (5) in Fig. 10) were very small (0.0017 and 0.0000). In addition, the lack of overlapping between the two MOs in each transition made these transitions strongly forbidden. The values of oscillator strength (*f*) of the $S_2 \rightarrow S_0$ transitions at $R^{EES(S2)}$ and $R^{EES(S1)}$ (process (4) and (6) in Fig. 10) were very large (0.5156 and 0.3777). In addition,

there was an overlapping of the MOs in these transitions. These results showed that the $S_2 \rightarrow S_0$ transitions at $R^{EES(S2)}$ and $R^{EES(S1)}$ occurred in structure (III). The calculated fluorescence energies of these transitions (in the ethanol solution) were 3.64 and 3.82 eV, a difference of about 0.89 and 0.51 eV compared with the previously published data. The value of oscillator strength (*f*) of the $S_2 \rightarrow S_0$ transition at $R^{EES(S2)}$ was larger than that at $R^{EES(S1)}$. In addition, the geometry of the S_2 state at $R^{EES(S1)}$ was not optimized yet. It quickly goes to the optimized geometry at $R^{EES(S2)}$. This is why the fluorescence intensity at a long wavelength was much stronger than that at a short wavelength in the experiments [3].

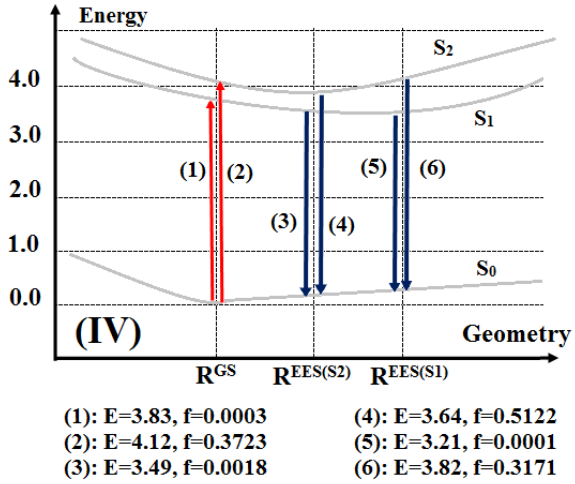

Fig. 10. Energy diagram of the excitation and emission processes of (IV) at R^{GS}, $R^{EES(S1)}$ and $R^{EES(S2)}$

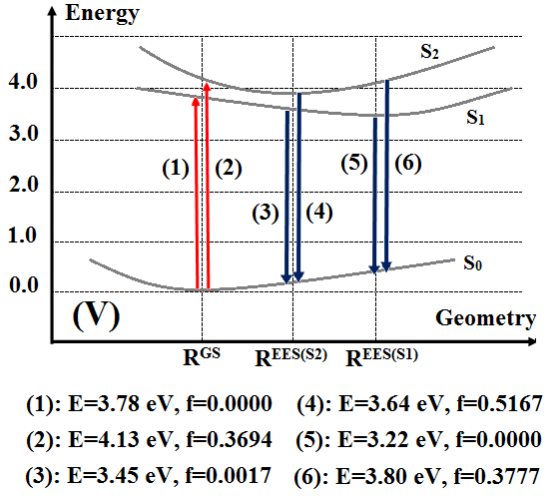

Fig. 11. Energy diagram of the excitation and emission processes of (V) at R^{GS}, $R^{EES(S1)}$ and $R^{EES(S2)}$

The calculated results from structures (V) were completely similar to those from structure (IV). The $S_0 \rightarrow S_2$ transition (process (2) in Fig. 11) was a main singlet electronic transition from GS to EES. The calculated vertical excitation energy of the $S_0 \rightarrow S_2$ transition (in the ethanol solution) was 4.13 eV, a difference of about 0.26 eV compared with the previously published data [3]. The $S_1 \rightarrow S_0$ transitions at $R^{EES(S2)}$ and $R^{EES(S1)}$ (process (3) and (5) in Fig. 11) were strongly forbidden. The $S_2 \rightarrow S_0$ transitions at $R^{EES(S2)}$ and $R^{EES(S1)}$ were main singlet electronic transitions from EES to GS. The calculated fluorescence energies of these transitions (in the ethanol solution) were 3.64 and 3.80 eV, a difference of about 0.89 and 0.50 eV compared with the previously published data [3]. The cause of the fluorescence intensity of structure (V) at a long wavelength being much stronger than that at a short wavelength was also explained in a similar way for structure (IV).

For structures (III), (IV) and (V), the calculated results indicated that the fluorescence occurred from the higher-electronic excited state (S_2) instead of occurring from the lowest-electronic excited state (S_1) as in other common cases. This is one of the exceptions from Kasha's rule. In this case, the energy gap between S_2 and S_1 was small; the oscillator strength of the $S_0 \rightarrow S_2$ transition was large, but the oscillator strength of the $S_0 \rightarrow S_1$ transition was small. These factors caused a long lifetime of the S_1 state. As a result, the fluorescence occurred from the S_2 state [21]. The fluorescence from the S_2 state could also be explained from the optimized geometries of the S_0, S_1, S_2 states of structures (III), (IV) and (V). The dihedral angle twisting between the coumarin and acryloxy moieties in structure (III) at $R^{EES(S1)}$ and $R^{EES(S2)}$, structure (IV) and (V) at $R^{EES(S1)}$ made the π-electron conjugated system broken, leading to the strong separation of electron density between the coumarin and acryloxy moieties. As a result, the lack of overlapping between two MOs in each transition made the $S_1 \rightarrow S_0$ and $S_2 \rightarrow S_0$ transitions in structure (III), the $S_1 \rightarrow S_0$ transition in the structure (IV) and (V) forbidden or negligible. Meanwhile, the coumarin moiety and acryloxy moiety in structure (IV) and (V) at $R^{EES(S2)}$ were coplanar. This is the favourable factor for overlapping between two MOs in the $S_2 \rightarrow S_0$ transitions in structure (IV) and (V). As a result, the fluorescence emission was from the S_2 excited state.

4 Conclusions

The DFT and TD-DFT methods with the B3LYP functional and LanL2DZ basis set were used for the investigation of the excitation and emission properties of some fluorophores with reliable results. In general, the optical properties had a good agreement between experiments and calculations, except for the absolute values of energies. The calculated energies were often larger than the experimental ones. This large deviation occurred when there were great variations between the optimized geometries of the ground state and the excited states, such as in structures (III), (IV) and (V). They could be due to the presence of the solvent components in a real solution that stabilized the excited states, leading to reduce the excitation and emission energies in the experiments. These differences could be reduced

in subsequent studies by looking for another level of theory that is more appropriate than the B3LYP/LanL2DZ level of theory.

Acknowledgements

This research was funded by the Vietnam National Foundation for Science and Technology Development (NAFOSTED) under grant number 104.06-2016.32.

References

1. Juan CS, Alfonso BC (2017). *Fluorescence Microscopy in Life Sciences*. Bentham Science Publishers, ISBN 978-1-68108-519-7.
2. Bernard V (2001). *Molecular Fluorescence: Principles and Applications*. Wiley-VCH Verlag GmbH, Weinheim – New York – Chichester – Brisbane – Singapore – Toronto, ISBN 3-527-29919-X.
3. Hien NK, Nhan DT, Kim WY, Bay MV, Nam PC, Van DU, Lim IT, Kim JS, Quang DT (2018). Exceptional case of Kasha's rule: Emission from higher-lying singlet electron excited states into ground states in coumarin-based biothiol sensing. *Dyes and Pigments*, 152, 118–126.
4. Nhan DT, Hien NK, Duc HV, Nhung TNA, Trung NT, Van DU, Shin WS, Kim JS, and Quang DT (2016). A hemicyanine complex for the detection of thiol biomolecules by fluorescence. *Dyes and Pigments*, 131, 301–306.
5. Godbey WT (2014). *An Introduction to Biotechnology: The Science, Technology and Medical Applications*. Academic Press, ISBN: 978-1-907568-28-2.
6. Shahzad A, Köhler G, Knapp M, Gaubitzer E, Puchinger M, and Edetsberger M (2009). Emerging applications of fluorescence spectroscopy in medical microbiology field. *Journal of Translational Medicine*, 7: 99.
7. Dai HQ, Tri NN, Trang NTT, Trung NT (2014). Remarkable effects of substitution on stability of complexes and origin of the C–H···O(N) hydrogen bonds formed between acetone's derivative and CO_2, XCN (X = F, Cl, Br). *Royal Society of Chemistry Advances*, 4, 13901–13908.
8. Karabacak M, Cinar M, Kurt M, Poiyamozhi A, Sundaraganesan N (2014). The spectroscopic (FT-IR, FT-Raman, UV and NMR) first-order hyperpolarizability and HOMO–LUMO analysis of dansyl chloride. *Spectrochimica Acta Part A: Molecular and Biomolecular Spectroscopy*, 117, 234–244.
9. Keawwangchai T, Morakot N, Wanno B (2013). Fluorescent sensors based on BODIPY derivatives for aluminium ion recognition: an experimental and theoretical study. *Journal of Molecular Modeling*, 19(3), 1435–1444.
10. Keawwangchai T, Wanno B, Morakot N, Keawwangchai S (2013). Optical chemosensors for Cu(II) ion based on BODIPY derivatives: an experimental and theoretical study. *Journal of Molecular Modeling*, 19(10), 4239–4249.
11. Frisch MJ et al (2009). *Gaussian 09*, Revision E.01. Wallingford CT: Gaussian Inc.

12. Hien NK, Bao NC, Nhung NTA, Trung NT, Nam PC, Duong T, Kim JS, Quang DT (2015). A highly sensitive fluorescent chemosensor for simultaneous determination of Ag(I), Hg(II), and Cu(II) ions: Design, synthesis, characterization and application. *Dyes and Pigments,* 116, 89–96.
13. Nhan DT, Nhung NTA, Vien V, Trung NT, Cuong ND, Bao NC, Huong DQ, Hien NK, Quang DT (2017). A Benzothiazolium-derived colorimetric and fluorescent chemosensor for detection of Hg^{2+} ions. *Chemistry Letters*, 46(1), 135–138.
14. Stratmann RE, Scuseria GE, Frisch MJ (1998). An efficient implementation of time-dependent density-functional theory for the calculation of excitation energies of large molecules. *Journal of Chemical Physics*, 109(19), 8218–8224.
15. Carlo A, Denis J (2013). The calculations of excited-state properties with time-dependent density functional theory. *Chemical Society Reviews*, 42, 845–856.
16. Becke AD (1993). Density-functional thermochemistry. III. The role of exact exchange. *The Journal of Chemical Physics*, 98, 5648–5652.
17. Lee C, Yang W, Parr PG (1998). Development of the colle-salvetti correlation-energy formula into a functional of the electron density. *Phys Rev B Condens Matter*, 37(2), 785–789.
18. Zamojc K, Wiczk W, Zaborowski B, Jacewicz D, Chmurzynski L (2015). Fluorescence quenching of 7-amino-4-methylcoumarin by different TEMPO derivatives. *Spectrochimica Acta Part A: Molecular and Biomolecular Spectroscopy*, 136, 1875–1880.
19. Sherman WS and Robins E (1998). Fluorescence of substituted 7-hydroxycoumarins. *Analytical Chemistry*, 40(4), 803–805.
20. Sharma VK, Mohan D, Sahare PD (2007). Fluorescence quenching of 3-methyl 7-hydroxyl coumarin in presence of acetone. *Spectrochimica Acta Part A*, 66, 111–113.
21. Petr K, Jakob W (2009). *Photochemistry of organic compounds: from concepts to practice*. A John Wiley and Sons Ltd, United Kingdom.